Effect of *in situ* Sb doping on crystalline and electrical characteristics of n-type $Ge_{1-x}Sn_x$ epitaxial layer

Jihee Jeon[1], Takanori Asano[1, 2], Yosuke Shimura[1], Wakana Takeuchi[1], Masashi Kurosawa[1, 3], Mitsuo Sakashita[1], Osamu Nakatsuka[1], and Shigeaki Zaima[1, 3]

[1]*Department of Crystalline Materials Science, Graduate School of Engineering, Nagoya University, Nagoya 464-8603, Japan*
[2]*Research Fellow of the Japan Society for the Promotion of Science, Japan*
[3]*Institute of Materials and Systems for Sustainability, Nagoya University, Nagoya 464-8603, Japan*

*E-mail: jjeon@alice.xtal.nagoya-u.ac.jp

We examined the molecular beam epitaxy of $Ge_{1-x}Sn_x$ with *in situ* Sb doping on Ge substrates. The effects of Sb doping on the crystalline and electrical characteristics of $Ge_{1-x}Sn_x$ epitaxial layer were investigated in detail. We found that Sb doping with a concentration of 10^{20} cm^{-3} remarkably improves the crystallinity, and surface uniformity of the $Ge_{1-x}Sn_x$ epitaxial layer by changing the growth mode by the surfactant effect of Sb atoms. Low-temperature $Ge_{1-x}Sn_x$ growth with *in situ* Sb doping realizes a very high electron concentration of 10^{20} cm^{-3}, which is above the thermal equilibrium solid solubility, as a result of suppressing Sb segregation and precipitation.

1. Introduction

Ge is a promising channel material for next-generation metal-oxide-semiconductor field effect transistors (MOSFETs) because of its theoretically predicted higher electron and hole mobilities than those of Si. In addition, Ge, a group-IV material, is applicable to the state-of-the-art Si process, and it is relatively easy to introduce Ge into conventional Si integrated circuits.

Considering practical applications, not only p-MOSFET but also n-MOSFET is required for low power-consumption complementary MOS. One of the challenges in improving Ge n-MOSFET is the use of strain technology; a theoretical calculation predicts that the electron mobility can be enhanced with uniaxial compressive strain along the $[\bar{1}\bar{1}0]$ direction [1]. A uniaxial strain can be applied by using the lattice constant difference between channel and source/drain (S/D) regions [2,3]. To realize a uniaxial compressive strained Ge channel n-MOSFET with a high mobility, we are considering n^+-$Ge_{1-x}Sn_x$ S/D stressors as well as p-MOSFETs [3]. Moreover, by taking advantage of the atomic radius of Sn (1.45 Å), which is larger than that of Ge (1.25 Å), the lattice constant of the $Ge_{1-x}Sn_x$ layer can be controlled by adjusting the Sn content, which enables the control of the magnitude of the local strain in the Ge channel [3-5].

Here, we need to deal with some requirements for realizing $Ge_{1-x}Sn_x$ S/D applications. First, the $Ge_{1-x}Sn_x$ stressor needs a high Sn content; a Sn content of more than 6% can induce large stress in the channel (as large as 1.4 GPa), resulting in a 2-fold mobility enhancement [1,3]. For applications, the $Ge_{1-x}Sn_x$ layer should be epitaxially grown without dislocations at the interface with Ge to suppress the junction leakage current. The large lattice mismatch and the low solid solubility of Sn in Ge cause difficulties in the epitaxial growth of $Ge_{1-x}Sn_x$ with a high Sn content and in the suppression of Sn precipitation and threading dislocations. It is now known that the high Sn content, which exceeds the solid solubility limit, can be achieved by nonequilibrium growth such as low-temperature molecular beam epitaxy (MBE) [6].

Second, heavy doping technology for the $Ge_{1-x}Sn_x$ layer as source/drain with an electron concentration as high as 10^{20} cm^{-3} should be developed for lowering the parasitic resistance [7]. However, heavy n-type doping technology even for Ge is still under development because heavy n-type doping on Ge is generally difficult owing to the low solid solubility and the low activation ratio of group-V dopants such as phosphorus, arsenic, and antimony in Ge [8-15]. The other concern is the segregation of dopant atoms during the growth of $Ge_{1-x}Sn_x$, resulting in a nonuniform profile.

To overcome these difficulties, we focused on the *in situ* doping and low-temperature epitaxy of the $Ge_{1-x}Sn_x$ layer under nonthermal equilibrium condition. Among the other group-V materials as n-type dopant for the $Ge_{1-x}Sn_x$ layer, Sb has a fascinating advantage of surfactant effect, which suppresses the three-dimensional island growth and realizes a smooth surface and an abrupt interface during epitaxial growth [16-18]. *In situ* doping is a well-known damage-free doping technique compared with conventional ion implantation. Meanwhile, both low-temperature growth and nonthermal equilibrium condition can counteract the low solid solubility, as well as Sn alloying in the Ge matrix.

Therefore, the control of Sb segregation and incorporation in the $Ge_{1-x}Sn_x$ layer during the *in situ* nonthermal equilibrium growth has the possibility realizing both heavy doping and high crystallinity. However, there are few reports of *in situ* Sb heavy doping in $Ge_{1-x}Sn_x$ epitaxy and the effect of Sb on the epitaxial growth and electrical property of the $Ge_{1-x}Sn_x$ layer. In this study, we examined *in situ* Sb doping during $Ge_{1-x}Sn_x$ epitaxy on Ge substrate for the formation of a heavily doped n-type $Ge_{1-x}Sn_x$ epitaxial layer with an Sb concentration above 10^{20} cm^{-3}, which is higher than the Sb solid solubility of 10^{19} cm^{-3} in Ge. We also investigated the effect of Sb doping on the crystallinity and electrical properties of $Ge_{1-x}Sn_x$ epitaxial layers.

2. Experimental procedure

A p-type Ge(001) wafer was used as the substrate. Each substrate was rinsed in deionized water (DIW). Then, the substrate was chemically cleaned by dipping in aqueous ammonia solution ($NH_4OH:H_2O=1:4$) for 5 min. After rinsing the substrate with DIW, it was dipped in sulfuric acid solution ($H_2SO_4:H_2O=1:7$) for 2 min. Finally, the substrate was rinsed with DIW and dried by N_2 blowing. The chemical oxide layer on the Ge substrate was removed by thermal treatment at 430 °C for 30 min in an ultrahigh vacuum (UHV) MBE chamber with a base pressure of less than 10^{-7} Pa. An Sb-doped $Ge_{1-x}Sn_x$ layer was grown on a substrate at 150 °C. Ge, Sn, and Sb were simultaneously deposited with individual Knudsen cells (K-cells). The thickness of $Ge_{1-x}Sn_x$ layers on the Ge(001) substrate was 100 nm. The target Sn content in $Ge_{1-x}Sn_x$ was 6% by controlling the temperatures of Ge and Sn Knudsen cells. The Sb concentration was increased to the order of 10^{20} cm^{-3} by increasing the K-cell temperature to 280 °C. For comparision, undoped $Ge_{1-x}Sn_x$ and Sb-doped Ge epitaxial layers were also prepared with all the other growth conditions being the same. To look over the growth aspect of *in situ* Sb-doped Ge and $Ge_{1-x}Sn_x$ samples and the chemical concentration of Sb, secondary ion mass spectrometry (SIMS) measurement was performed. The vapor pressure of Sb in our MBE system was calibrated on the basis of SIMS results and we expected the Sb concentration by calculating vapor pressure from the Sb K-cell temperature. The Sb concentration was controlled in the range of 10^{18}, 10^{19}, and 10^{20} cm^{-3} by changing the K-cell temperatures to 220, 250, and 280 °C, respectively.

X-ray diffraction two-dimensional reciprocal space mapping (XRD-2DRSM; PANalytical MRD Pro) with a CuKα X-ray source was carried out to characterize the crystalline structure of Sb-doped $Ge_{1-x}Sn_x$ layers. The substitutional Sn contents in the $Ge_{1-x}Sn_x$ layers were estimated by measuring the distance between $Ge_{1-x}Sn_x\bar{2}\bar{2}4$ and Ge $\bar{2}\bar{2}4$ reciprocal lattice points in XRD-2DRSM results. Atomic force microscopy (AFM; JEOL JSPM4200) was used to observe the surface morphologies of $Ge_{1-x}Sn_x$ layers. Furthermore, micro four-point probe (M4PP; CAPRES microRSP-M200) and

micro-Hall effect (MHE) measurements were performed to characterize the electrical properties of the Sb-doped $Ge_{1-x}Sn_x$ layers.

3. Results and discussion

Figures 1(a)-1(d) show the *in situ* reflection high-energy electron diffraction (RHEED) patterns of surfaces of $Ge_{1-x}Sn_x$ and $Ge_{1-x}Sn_x$:Sb layers grown on Ge substrates immediately after the epitaxial growth. A spot pattern is observed for the undoped $Ge_{1-x}Sn_x$ layer without Sb due to the three-dimensional growth mode of $Ge_{1-x}Sn_x$ epitaxy on Ge, as shown in Fig. 1(a). On the other hand, the spot pattern gradually changes to a streak pattern with increasing Sb concentration, as shown in Figs. 1(b)-1(c). Finally, for the Sb-doped $Ge_{1-x}Sn_x$ layer with an Sb K-cell temperature of 280 °C, the RHEED pattern shows a sharp streak [Fig. 1(d)]. This result indicates that increasing the *in situ* doping concentration of Sb modifies the growth mode of the $Ge_{1-x}Sn_x$ layer and effectively improves the crystalline quality of the epitaxial layer.

Figures 2(a) and 2(b) show the SIMS depth profiles for Ge:Sb(280 °C)/Ge and $Ge_{1-x}Sn_x$:Sb(280 °C)/Ge samples. We evaluated the depth profiles of Ge, Sn, and Sb atoms. In Fig. 2(a), a uniform depth profile of Sb was achieved with a concentration as high as 2.3×10^{20} cm^{-3}, which is relatively higher than the Sb thermal equilibrium solid solubility of 10^{19} cm^{-3} in the Ge matrix. Also, in Fig. 2(b), uniform depth profiles of Sb and Sn were achieved. Since the Sn solid solubility in Ge matrix is 1%, an Sb concentration of 2×10^{20} cm^{-3} and a Sn content of 6% in $Ge_{1-x}Sn_x$:Sb (280 °C) are both higher than the solid solubility in Ge. We considered that the low-temperature growth under nonthermal equilibrium condition effectively suppresses Sb segregation during the epitaxy and gives the high Sb and Sn concentrations over the solubility limit in Ge.

Figures 3(a)-3(d) show XRD-2DRSM results around the Ge $\bar{2}\bar{2}4$ Bragg reflection for

$Ge_{1-x}Sn_x$/Ge samples without Sb and with Sb deposited at K-cell temperatures of 220, 250, and 280 °C, respectively. The reciprocal lattice Q_x value of the diffraction peak related to the $Ge_{1-x}Sn_x$:Sb epitaxial layer is identical to that of Ge for all samples. This result indicates the pseudomorphic growth of the $Ge_{1-x}Sn_x$ epitaxial layer on the Ge substrate. The reciprocal lattice Q_y value of the Sb-doped $Ge_{1-x}Sn_x$ layer decreases, as seen in Figs. 3(a)-3(d), although the Ge and Sn fluxes for all samples are the same during the MBE growth. We confirmed that the Sn concentration in Ge was not affected depending on the Sb concentration by SIMS measurements for samples shown in Figs. 3(c) and 3(d) (*not shown*). Thus, the peak shift of $Ge_{1-x}Sn_x\bar{2}\bar{2}4$ reflection in XRD-2DRSM results for Sb-doped samples can be attributed to the Sb incorporation into the substitutional sites of $Ge_{1-x}Sn_x$, and Sb affects the lattice constant of the $Ge_{1-x}Sn_x$ epitaxial layer because the atomic radius of Sb is as large as that of Sn.

The substitutional Sn content of the undoped $Ge_{1-x}Sn_x$ layer was calculated to be 5.7% through the diffraction peak position of $Ge_{1-x}Sn_x\bar{2}\bar{2}4$, assuming the elastic deformation and Vegard's law.

$$a_{GeSn}(x) = (1-x)a_{Ge} + xa_{Sn}, \quad (1)$$

Here a_{Ge} and a_{Sn} are the lattice constants of bulk Ge (5.6579 Å) and bulk Sn (6.4892 Å), respectively [19], and we can estimate the lattice constant a_{GeSn} of $Ge_{1-x}Sn_x$ with a Sn content. The lattice constant along the [001] direction of a $Ge_{1-x}Sn_x$ layer pseudomorphically grown on Ge [001] $a_{[001]}$ is expressed using the Poisson ratio of $Ge_{1-x}Sn_x$ ν_{GeSn}: [20]

$$a_{[001]} = \frac{1+\nu_{GeSn}}{1-\nu_{GeSn}} a_{GeSn} - \frac{2\nu_{GeSn}}{1-\nu_{GeSn}} a_{Ge}. \quad (2)$$

ν_{GeSn} can be approximately estimated by a linear relationship using Ge's Poisson ratio (=0.273) and Sn's Poisson ratio (=0.356).

The magnified logarithm peak profiles of the $Ge_{1-x}Sn_x\bar{2}\bar{2}4$ diffraction along the [110] direction are shown in Fig. 3(e). We can see that the $Ge_{1-x}Sn_x$/Ge sample with a higher Sb doping

concentration has a smaller broadening of the $Ge_{1-x}Sn_x$:Sb$\overline{2}\overline{2}4$ diffraction peak profile along the [110] direction. This means that the lattice fluctuation of the $Ge_{1-x}Sn_x\overline{2}\overline{2}4$ diffraction peak along the [110] direction improved with increasing Sb doping concentration, which would be due to the superior crystallinity of the Sb-doped $Ge_{1-x}Sn_x$ epitaxial layer. These RHEED and XRD results imply that the Sb doping strongly affects the crystallinity of $Ge_{1-x}Sn_x$:Sb epitaxial layers.

Figures 4(a)-4(d) show AFM images and surface profiles of $Ge_{1-x}Sn_x$ layers without Sb and with Sb deposited at K-cell temperatures of (b) 220 °C, (c) 250 °C, and (d) 280 °C. The undoped $Ge_{1-x}Sn_x$ layer without Sb shows a roughened surface, suggesting the Stranski-Krastanov growth mode. While the $Ge_{1-x}Sn_x$ layer with a low Sb concentration shows a similar surface morphology to the undoped one [Figs. 4(b) and 4(c)], increasing the Sb concentration to 10^{20} cm^{-3} provides a smooth and uniform surface of the $Ge_{1-x}Sn_x$ layer [Fig. 4(d)].

Figure 4(e) shows the Sb K-cell temperature dependence of the root-mean-square (RMS) roughness of Sb-doped Ge and $Ge_{1-x}Sn_x$ layers. The RMS roughness of the Ge surface without Sn does not change regardless of the Sb concentration, while the RMS roughness of the $Ge_{1-x}Sn_x$ surface monotonically decreases with increasing Sb concentration. Decreasing the RMS roughness of the $Ge_{1-x}Sn_x$ surface can be explained by the surfactant effect of Sb for epitaxial growth, which realizes a smooth surface and an abrupt interface. Above all, the $Ge_{1-x}Sn_x$:Sb (280 °C) sample had a lower RMS roughness than the Ge:Sb (280 °C) sample. Therefore, we could say that the surfactant effect appears with a sufficiently high Sb concentration.

Next, we investigated the electrical properties of these Sb-doped $Ge_{1-x}Sn_x$ and Ge epitaxial layers. Figure 5 demonstrates the decrease in the sheet resistance of the Sb-doped $Ge_{1-x}Sn_x$ epitaxial layer as a function of Sb K-cell temperature. The sheet resistance was measured by using M4PP. This result indicates the increase in the electron concentration with the Sb doping concentration. Although

the sheet resistance of the $Ge_{1-x}Sn_x$ layer with a low Sb doping concentration is about 5 times higher than that of the Sb-doped Ge layer, the difference in the sheet resistance between $Ge_{1-x}Sn_x$ and Ge decreases for samples with Sb doping concentrations as high as 10^{20} cm^{-3}.

The relationship between the Hall electron mobility and the carrier concentration is revealed by MHE measurement as shown in Fig. 6. Electron concentrations as high as 1.5×10^{20} and 1.4×10^{20} cm^{-3} were obtained in Ge:Sb and $Ge_{1-x}Sn_x$:Sb samples, respectively. Previously, it was reported that the Ge:P epitaxial layer prepared by low-pressure chemical vapor deposition with a growth temperature of 320 °C achieved a carrier concentration of 6.2×10^{19} cm^{-3} [21,22]. In this study, electron concentrations much higher than the previously reported values are obtained in not only the Sb-doped Ge epitaxial layer but also the Sb-doped $Ge_{1-x}Sn_x$ one. It is considered that the low-temperature growth of the *in situ* Sb-doped $Ge_{1-x}Sn_x$ epitaxial layer at as low as 150 °C achieves heavy n-type doping over the thermal equilibrium solid solubility limit of Sb.

In addition, we observed that mobility increases even with increasing carrier concentration, as shown in Fig. 6. There are two convincing explanations for this enhancement. First is the crystallinity improvement of the epitaxial layers due to the Sb surfactant effect, as we showed above. Second is the parallel conduction both in L and gamma valleys. Because of the high carrier concentration, the Fermi level could be pushed over the gamma valley, resulting in the electron occupation both in the gamma and L valleys [23,24]. As a result of the small effective mass for the gamma valley [25], the sample with higher carrier concentration has a higher net mobility. Indeed, in the case of the Ge:Sb sample with the electron concentration of 1×10^{20} cm^{-3} , the amount of electron at the gamma valley is relatively low because the Fermi level is only slightly higher than the gamma valley. However, in the case of the Ge:Sb sample with the electron concentration of 1.5×10^{20} cm^{-3}, the contribution of conduction at the gamma valley to the parallel conduction is higher owing to the higher electron concentration in the gamma valley. Therefore, the net mobility is higher.

Note that the mobility of our Ge:Sb exceeds that of the heavily doped bulk Ge [26]. The reference data, however, shows the possibility of a poor-quality Ge wafer. Actually, a superior electrical property is reported for p-type Ge in Refs. [27,28]. We achieved heavy n-type doping, which has not been attempted so far, exceeding the carrier concentration range of bulk n-type Ge reference around 10^{15}- 10^{19} cm^{-3}. In addition, a lower mobility of $Ge_{1-x}Sn_x$ than Ge could mainly be due to the mobility reduction effect with biaxial compressive strain in the $Ge_{1-x}Sn_x$ epitaxial layer pseudomorphically grown on Ge.

The activation ratio of Sb as n-type carrier was estimated as an n-type carrier concentration from MHE measurement divided by the Sb chemical concentration estimated by SIMS measurement. The activation ratio of Sb in the $Ge_{1-x}Sn_x$:Sb(280 °C)/Ge sample reached 69%, which is as high as that of 65% in the Ge:Sb(280 °C)/Ge sample.

4. Conclusions

In situ Sb doping in the $Ge_{1-x}Sn_x$ epitaxial layer under nonthermal equilibrium condition was examined to realize heavy doping of Sb. The effects of Sb doping on the crystalline and electrical properties of the $Ge_{1-x}Sn_x$ epitaxial layer were systematically investigated. From XRD-2DRSM results, decreasing the broadening of the $Ge_{1-x}Sn_x\bar{2}\bar{2}4$ diffraction peak profile along the $[\bar{1}\bar{1}0]$ direction indicates the high crystallinity of the heavily Sb-doped $Ge_{1-x}Sn_x$ epitaxial layer. RHEED and AFM measurements reveal that the surfactant effect of Sb effectively improves the uniformity and flatness of the $Ge_{1-x}Sn_x$ epitaxial layer. The surfactant effect significantly appears with a sufficiently high Sb concentration of about 10^{20} cm^{-3}.

The electrical property was examined by M4PP and MHE measurements for the Sb-doped $Ge_{1-x}Sn_x$ epitaxial layer. High electron concentrations of 1.5×10^{20} and 1.4×10^{20} cm^{-3} were achieved in Ge:Sb and $Ge_{1-x}Sn_x$:Sb samples, respectively, which promises high performance of n-type

$Ge_{1-x}Sn_x$ electronic applications. We also observed that mobility increases with increasing carrier concentration owing to the crystallinity improvement with Sb doping. The activation ratio as high as 69% is achieved in the $Ge_{1-x}Sn_x$:Sb sample; moreover, this value is higher than that of the Ge:Sb sample. As a result, we can say that *in situ* Sb-doping under nonthermal equilibrium condition has a promising possibility for realizing heavy doping with superior crystallinity of the $Ge_{1-x}Sn_x$ epitaxial layer.

Acknowledgements

This work was partly supported by a Grant-in-Aid for Scientific Research (S) (No. 26220605) and (B) (No. 15H03565) from the Japan Society for the Promotion of Science. We would also like to thank Dr. R. Loo, Dr. J. Bogdanowicz, and Dr. B. Parmentier of the IMEC, Belgium, for their assistance with the micro-Hall effect measurements.

References

[1] Y. -J. Yang, W. S. Ho, and C.-F. Huang, Appl. Phys. Lett. **91**, 102103 (2007).

[2] T. Ghani, M. Armstrong, C. Auth, M. Bost, P. Charvat, G. Glass, T. Hoffmann, K. Johnson, C. Kenyon, J. Klaus, B. McIntyre, K. Mistry, A. Murthy, J. Sandford, M. Silberstein, S. Sivakumar, P. Smith, K. Zawadzki, S. Thompson, and M. Bohr, IEDM Tech. Dig., 2003, p. 11.6.1.

[3] B. Vincent, Y. Shimura, S. Takeuchi, T. Nishimura, G. Eneman, A. Firrincieli, J. Demeulemeester, A. Vantomme, T. Clarysse, O. Nakatsuka, S. Zaima, J. Dekoster, M. Caymax, and R. Loo, Microelectron. Eng. **88**, 342 (2011).

[4] S. Ike, Y. Moriyama, M. Kurosawa, N. Taoka, O. Nakatsuka, Y. Imai, S. Kimura, T. Tezuka, and S. Zaima, Thin Solid Films **557**, 164 (2014).

[5] S. Ike, O. Nakatsuka, Y. Moriyama, M. Kurosawa, N. Taoka, Y. Imai, S. Kimura, T. Tezuka, and S. Zaima, Appl. Phys. Lett. **106**, 182104 (2015).

[6] O. Nakatsuka, N. Taoka, T. Asano, T. Yamaha, M. Kurosawa, M. Sakashita, and S. Zaima, ECS Trans. **58** [9], 149 (2013).

[7] H. Miyoshi, T. Ueno, Y. Hirota, J. Yamanaka, K. Arimoto, K. Nakagawa, and T. Kaitsuka, Jpn. J. Appl. Phys. **53**, 04EA05 (2014).

[8] K. Hozaki, M. Nakamura, Y. Shimura, W. Takeuchi, N. Taoka, O. Nakatsuka, and S. Zaima, Abstr. IUMRS-ICEM2012, 2012, p. B-1-O27-005.

[9] C. O. Chui, K. Gopalakrishnan, P. B. Griffin, J. D. Plummer, and K. C. Saraswat, Appl. Phys. Lett. **83**, 3275 (2003).

[10] C. O. Chui, Z. L. Kulig, J. Moran, and W. Tsai, Appl. Phys. Lett. **87**, 091909 (2005).

[11] M. Oehme, J. Werner, and E. Kasper, J. Cryst. Growth **310**, 4531 (2008).

[12] M. Takenaka, K. Morii, M. Sugiyama, Y. Nakano, and S. Takagi, Jpn. J. Appl. Phys. **50**, 010105 (2011).

[13] W. -K. Kim, K. Kuroda, M. Takenaka, and S. Takagi, IEEE Trans. Electron Devices **61**, 3379 (2014).

[14] G. Thareja, S.-L. Cheng, T. Kamins, K. Saraswat, and Y. Nishi, IEEE Electron Device Lett. **32**, 608 (2011).

[15] G. Thareja, S. Chopra, B. Adams, Y. Kim, S. Moffatt, K. Saraswat, and Y. Nishi, IEEE Electron Device Lett. **32**, 838 (2011).

[16] H. J. Osten, G. Lippert, and J. Klatt, J. Vac. Sci. Technol. B **10**, 1151 (1992).

[17] Th. Schmidt, R. Kröger, T. Clausen, J. Falta, A. Janzen, M. Kammler, P. Kury, P. Zahl, and M. Horn-von Hoegen, Appl. Phys. Lett. **86**, 111910 (2005).

[18] A. A. Tonkikh, and P. Werner, Phys. Status Solidi B, **250**, 1795 (2013).

[19] M. Oehme, J. Werner, M. Gollhofer, M. Schmid, M. Kaschel, E. Kasper, and J. Schulze, IEEE Photonics Technol. Lett. **23**, 1751 (2011).

[20] J. M. Hartmann, B. Gallas, J. Zhang, and J. J. Harris, Semicond. Sci. Technol. **15**, 370 (2000).

[21] Y. Shimura, S. A. Srinivasan, D. V. Thourhout, R. V. Deune, M. Pantouvaki, J. V. Campenhout, and R. Loo, to be published in Thin Solid Films.

[22] Y. Moriyama, Y. Kamimuta, Y. Kamata, K. Ikeda, A. Sakai, and T. Tezuka, Appl. Phys. Express **7**, 106501 (2014).

[23] X. Sun, J. Liu, L.C. Kimerling, and J. Michel, IEEE J. Sel. Top. Quantum Electron. **16**, 124 (2010).

[24] L. Carroll, P. Friedli, S. Neuenschwander, H. Sigg, S. Cecchi, F. Isa, D. Chrastina, G. Isella, Y. Fedoryshyn, and J. Faist, Phys. Rev. Lett. **109**, 057402 (2012).

[25] K. L. Low, Y. Yang, G. Han, W. Fan, and Y. -C. Yeo, J. Appl. Phys. **112**, 103715 (2012).

[26] V. I. Fistul, M. I. Iglitsyn, and E. M. Omelyanovskii, Sov. Phys. Solid State **4**, 784 (1962).

[27] O. A. Golikova, B. Ya. Moizhes, and L. S. Stil'bans, Sov. Phys. Solid State **3**, 3105 (1961).

[28] G. Impellizzeri, E. Napolitani, S. Boninelli, V. Privitera, T. Clarysse, W. Vandervorst, and F. Priolo, Appl. Phys. Express **5**, 021301 (2012).

Figure captions

Fig. 1. (Color online) RHEED patterns of $Ge_{1-x}Sn_x$ layers grown on Ge substrates **(a)** without Sb and with the Sb K-cell temperatures of **(b)** 220, **(c)** 250, and **(d)** 280 °C.

Fig. 2. (Color online) SIMS depth profiles of **(a)** Ge:Sb(280 °C)/Ge and **(b)** $Ge_{1-x}Sn_x$:Sb(280 °C)/Ge samples.

Fig. 3. (Color online) XRD-2DRSM results around the $Ge\overline{2}\overline{2}4$ Bragg reflection for $Ge_{1-x}Sn_x$/Ge samples **(a)** without Sb and with the Sb K-cell temperatures of **(b)** 220, **(c)** 250, and **(d)** 280 °C. **(e)** Magnified logarithm peak profiles of the $Ge_{1-x}Sn_x\overline{2}\overline{2}4$ diffraction along the [110] direction.

Fig. 4. (Color online) AFM images and surface profiles of $Ge_{1-x}Sn_x$ layers **(a)** without Sb and with Sb deposited at K-cell temperatures of **(b)** 220, **(c)** 250, and **(d)** 280 °C. **(e)** Sb concentration dependence of RMS roughness of Ge:Sb and $Ge_{1-x}Sn_x$:Sb layers.

Fig. 5. (Color online) Sb K-cell temperature dependence of sheet resistance for Ge:Sb and $Ge_{1-x}Sn_x$:Sb layers.

Fig. 6. (Color online) Carrier concentration dependence of Hall electron mobility for Ge:Sb and $Ge_{1-x}Sn_x$:Sb layers.

Figure 1

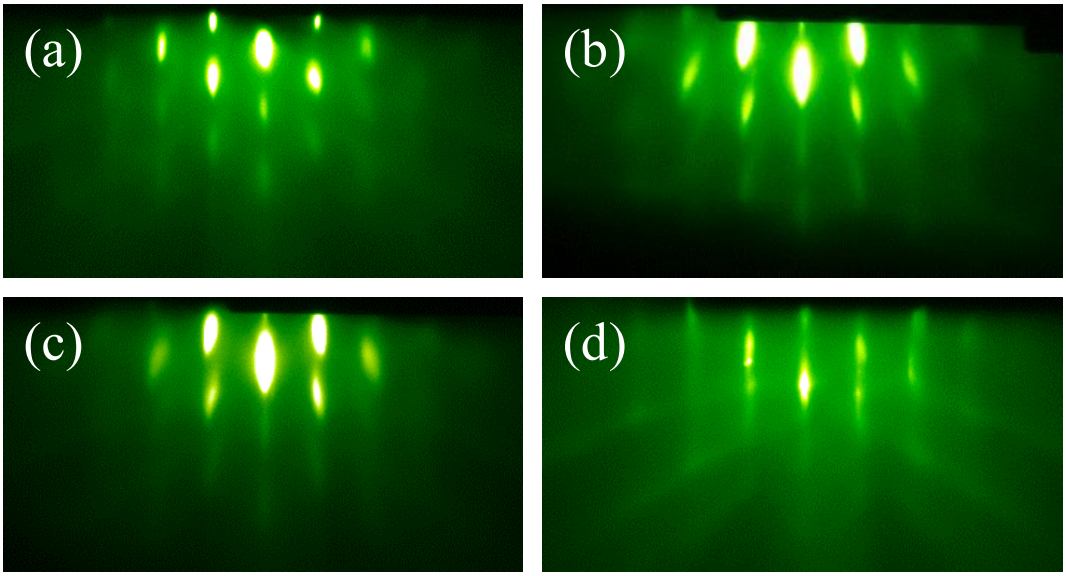

Figure 2

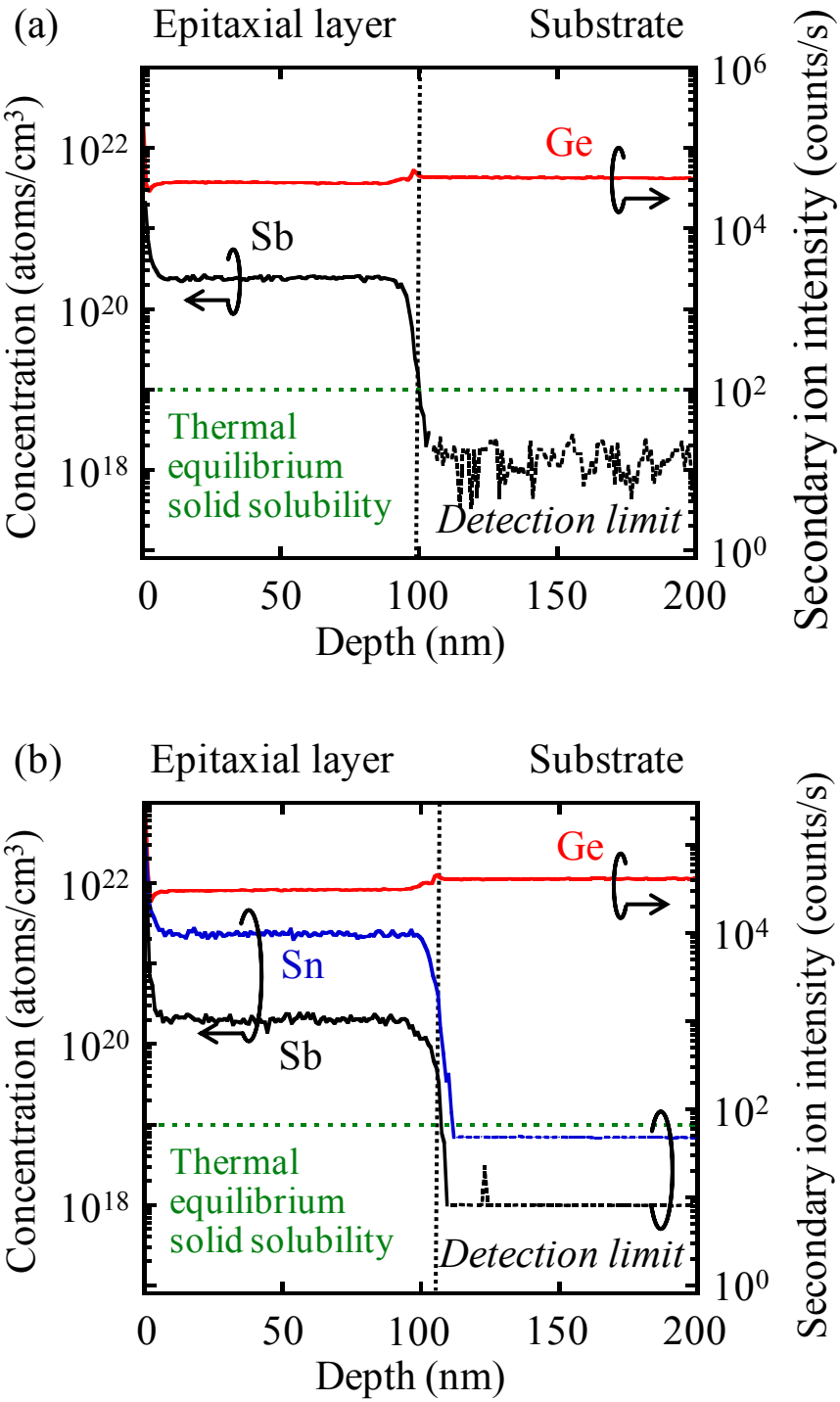
(a)
Epitaxial layer
Substrate
Ge
Sb
Thermal equilibrium solid solubility
Detection limit
Concentration (atoms/cm³)
Secondary ion intensity (counts/s)
Depth (nm)
(b)
Epitaxial layer
Substrate
Ge
Sn
Sb
Thermal equilibrium solid solubility
Detection limit
Concentration (atoms/cm³)
Secondary ion intensity (counts/s)
Depth (nm)

Figure 3

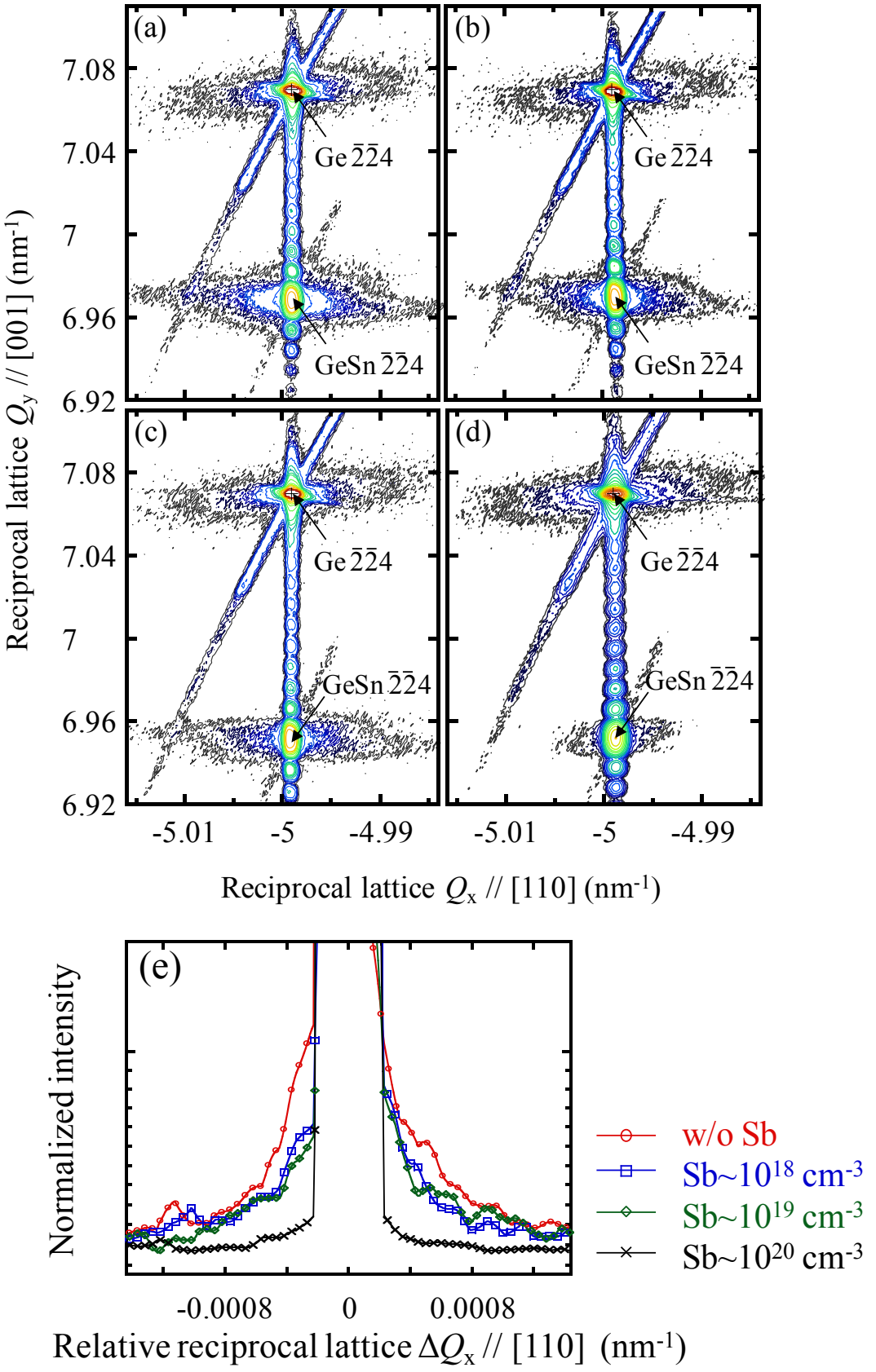
(a)
(b)
(c)
(d)
Ge $\bar{2}\bar{2}4$
GeSn $\bar{2}\bar{2}4$
7.08
7.04
7
6.96
6.92
-5.01
-5
-4.99
Reciprocal lattice Q_y // [001] (nm^{-1})
Reciprocal lattice Q_x // [110] (nm^{-1})
(e)
Normalized intensity
w/o Sb
Sb~10^{18} cm^{-3}
Sb~10^{19} cm^{-3}
Sb~10^{20} cm^{-3}
-0.0008
0
0.0008
Relative reciprocal lattice ΔQ_x // [110] (nm^{-1})

Figure 4

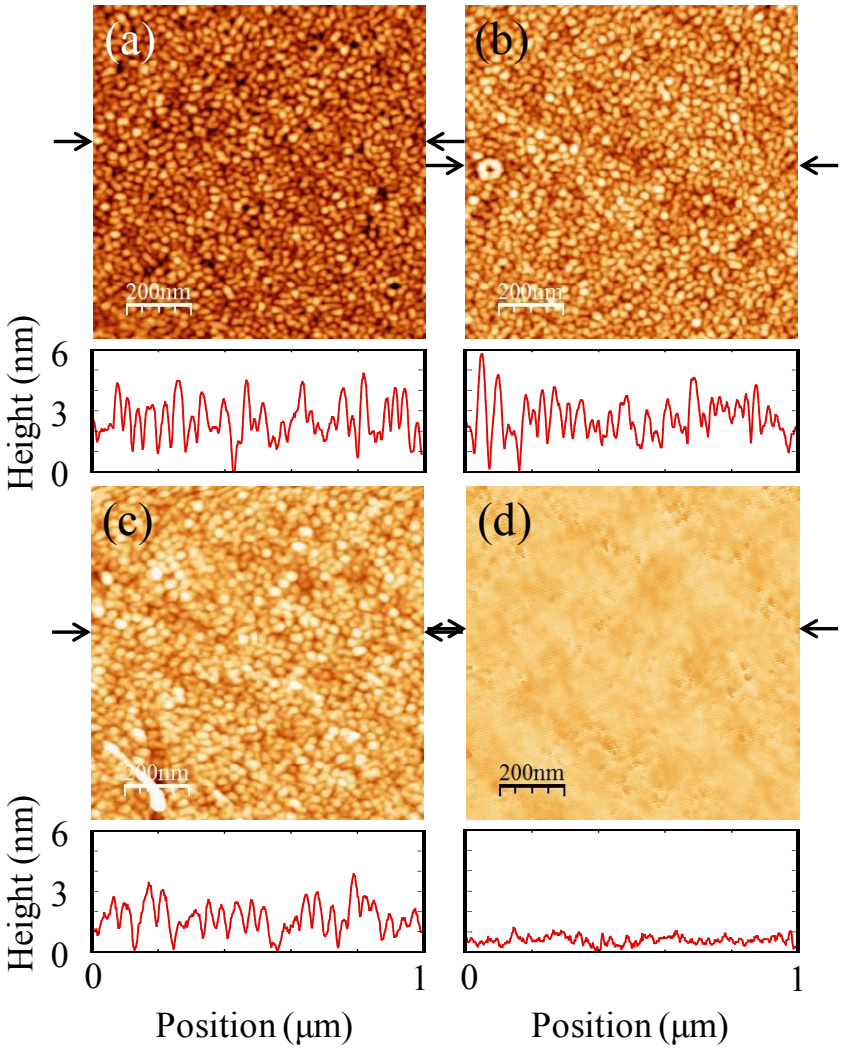
(a)
(b)
(c)
(d)
200nm
Height (nm)
6
3
0
0
1
Position (μm)

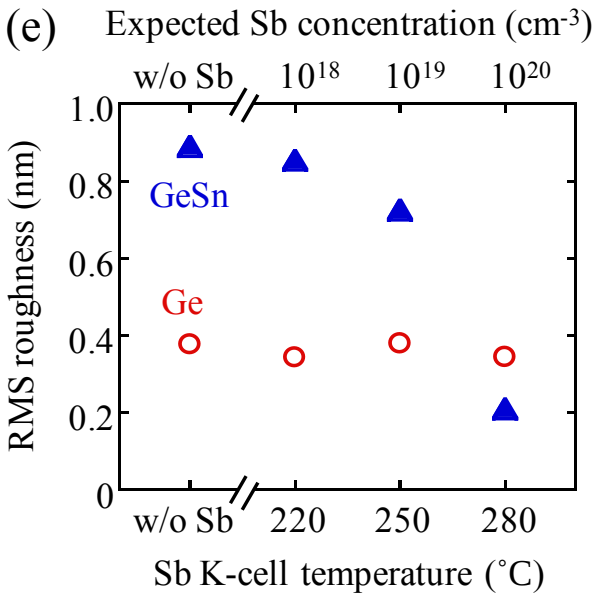
(e)
Expected Sb concentration (cm-3)
w/o Sb
10^18
10^19
10^20
RMS roughness (nm)
1.0
0.8
0.6
0.4
0.2
0
GeSn
Ge
w/o Sb
220
250
280
Sb K-cell temperature (˚C)

Figure 5

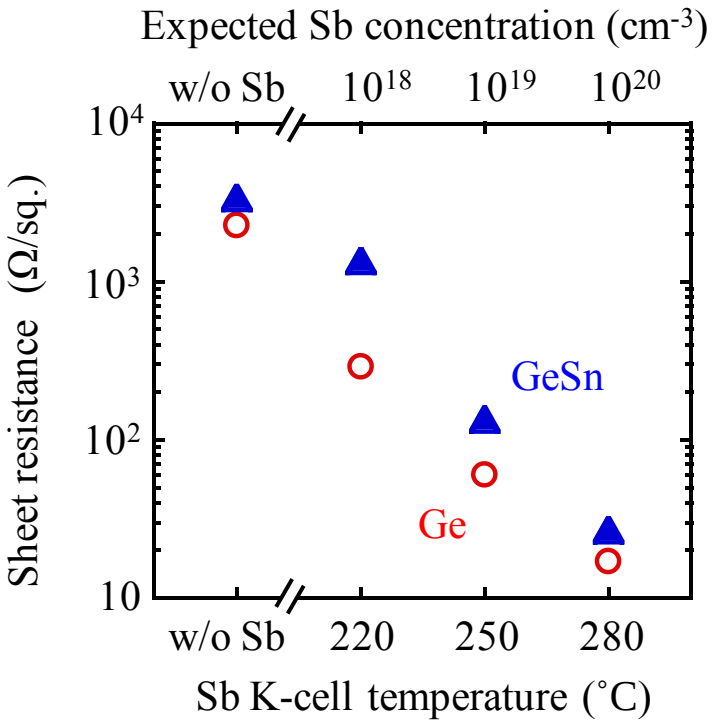
Expected Sb concentration (cm-3)
w/o Sb
10^18
10^19
10^20
10^4
10^3
10^2
10
Sheet resistance (Ω/sq.)
GeSn
Ge
w/o Sb
220
250
280
Sb K-cell temperature (˚C)

Figure 6

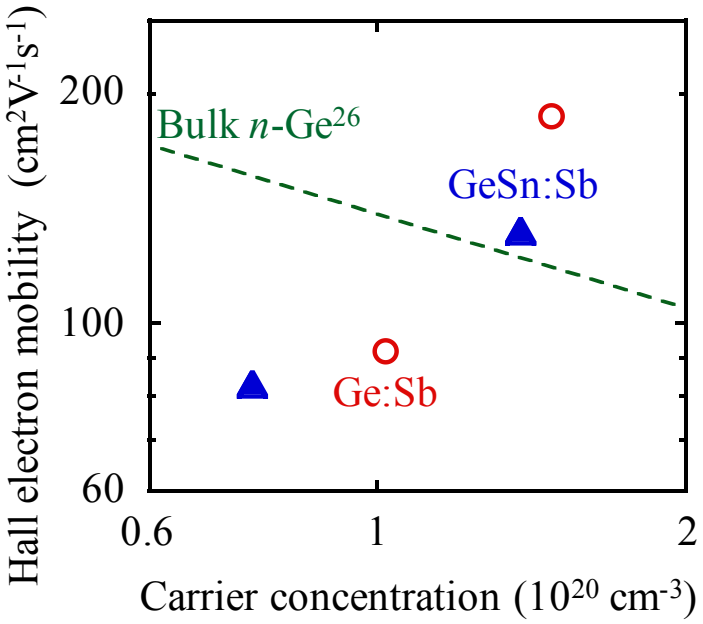
Hall electron mobility (cm²V⁻¹s⁻¹)
200
100
60
0.6
1
2
Carrier concentration (10²⁰ cm⁻³)
Bulk n-Ge[26]
GeSn:Sb
Ge:Sb

Figure 1(a) - 1(d)

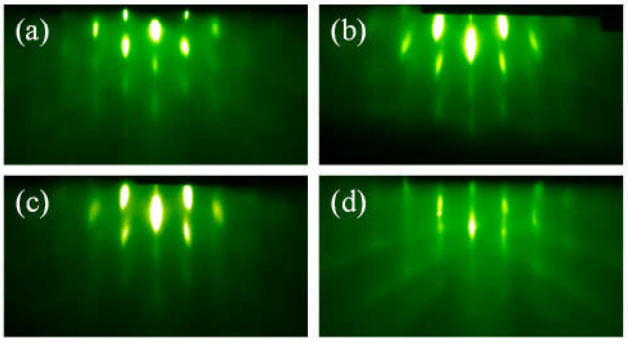

Figure 2(a) - 2(b)

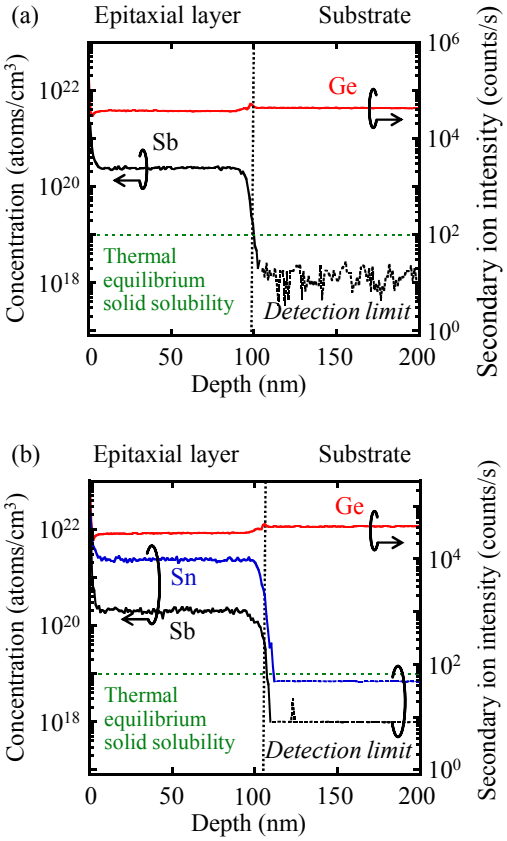
(a)
Epitaxial layer
Substrate
Ge
Sb
Thermal equilibrium solid solubility
Detection limit
Concentration (atoms/cm3)
Secondary ion intensity (counts/s)
Depth (nm)
(b)
Epitaxial layer
Substrate
Ge
Sn
Sb
Thermal equilibrium solid solubility
Detection limit
Concentration (atoms/cm3)
Secondary ion intensity (counts/s)
Depth (nm)

Figure 3(a) - 3(e)

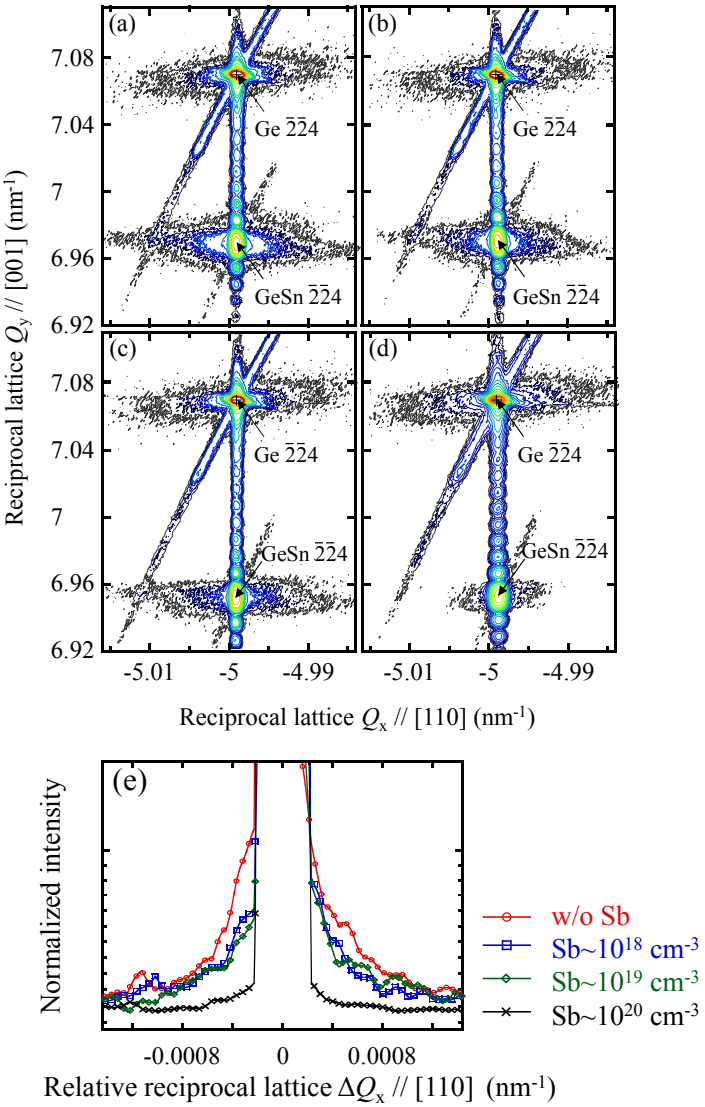
(a)
(b)
(c)
(d)
Ge $\bar{2}\bar{2}4$
GeSn $\bar{2}\bar{2}4$
7.08
7.04
7
6.96
6.92
-5.01
-5
-4.99
Reciprocal lattice Q_y // [001] (nm^{-1})
Reciprocal lattice Q_x // [110] (nm^{-1})
(e)
Normalized intensity
-0.0008
0
0.0008
Relative reciprocal lattice ΔQ_x // [110] (nm^{-1})
w/o Sb
Sb~10^{18} cm^{-3}
Sb~10^{19} cm^{-3}
Sb~10^{20} cm^{-3}

Figure 4(a) - 4(e)

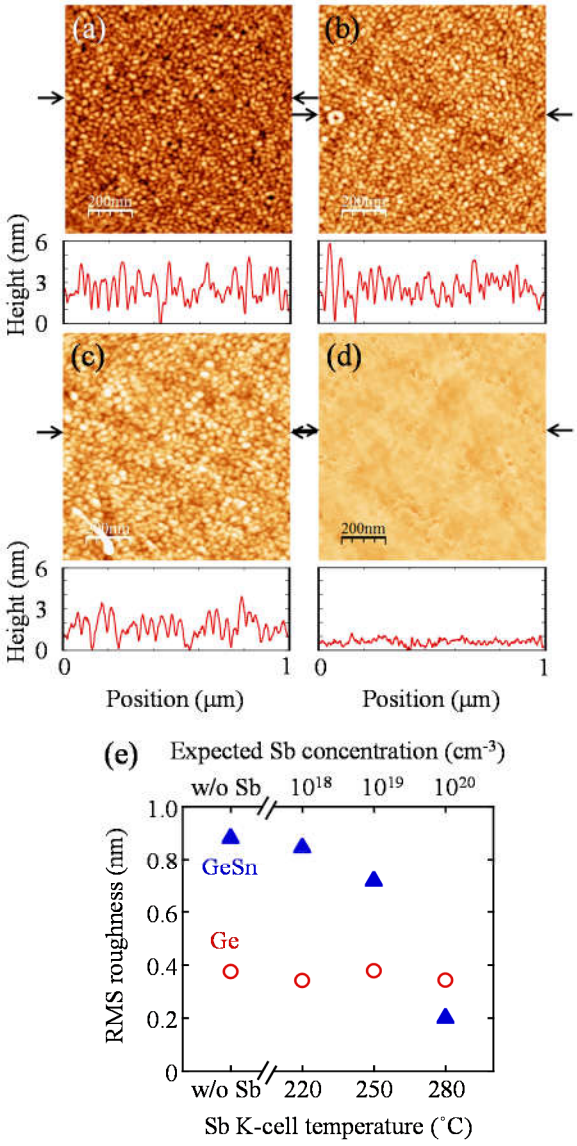
(a)
(b)
(c)
(d)
200nm
Height (nm)
6
3
0
0
1
Position (μm)
Position (μm)
(e)
Expected Sb concentration (cm-3)
w/o Sb
10^18
10^19
10^20
RMS roughness (nm)
1.0
0.8
0.6
0.4
0.2
0
GeSn
Ge
w/o Sb
220
250
280
Sb K-cell temperature (°C)

Figure 5

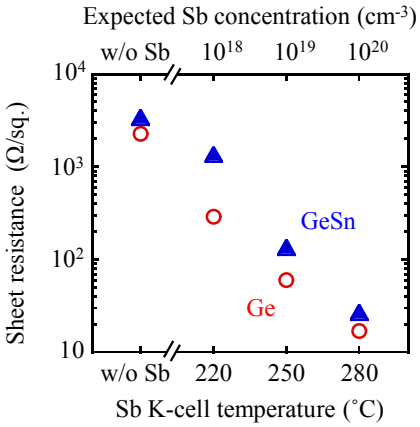
Expected Sb concentration (cm-3)
w/o Sb
10^18
10^19
10^20
10^4
10^3
10^2
10
Sheet resistance (Ω/sq.)
GeSn
Ge
w/o Sb
220
250
280
Sb K-cell temperature (˚C)

Figure 6

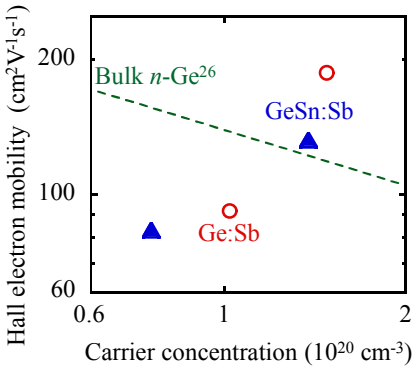
Hall electron mobility (cm²V⁻¹s⁻¹)
200
100
60
0.6
1
2
Carrier concentration (10²⁰ cm⁻³)
Bulk n-Ge[26]
GeSn:Sb
Ge:Sb